

Fine-tuning an ECG Foundation Model to Predict Coronary CT Angiography Outcomes

Yujie Xiao^{1,2,#}, Qinghao Zhao^{3,#}, Gongzheng Tang^{1,2}, Hao Zhang⁴, Zhuoran Kan^{1,2}, Deyun Zhang⁵, Jun Li^{1,2}, Guangkun Nie^{1,2,6}, Xiaocheng Fang^{1,2}, Haoyu Wang^{1,2,7}, Shun Huang^{1,2}, Tong Liu⁴, Jian Liu^{3,*}, Kangyin Chen^{4,*}, and Shenda Hong^{1,2,8,9,*}

¹Institute of Medical Technology, Peking University Health Science Center, Beijing, China

²National Institute of Health Data Science, Peking University, Beijing, China

³Department of Cardiology, Peking University People's Hospital, Beijing, China

⁴Tianjin Key Laboratory of Ionic-Molecular Function of Cardiovascular Disease, Department of Cardiology, Tianjin Institute of Cardiology, The Second Hospital of Tianjin Medical University, Tianjin, China

⁵Heart Voice Medical Technology, Hefei, China

⁶School of Intelligence Science and Technology, Peking University, Beijing, China

⁷University of Chinese Academy of Sciences, Beijing, China

⁸State Key Laboratory of Vascular Homeostasis and Remodeling, NHC Key Laboratory of Cardiovascular Molecular Biology and Regulatory Peptides, Peking University, Beijing, China

⁹Institute for Artificial Intelligence, Peking University, Beijing, China

#These authors contributed equally

*Correspondence: hongshenda@pku.edu.cn

Abstract

Coronary artery disease (CAD) remains a major global public health burden, yet scalable tools for risk screening are limited. Although coronary computed tomography angiography (CCTA) is a first-line non-invasive diagnostic modality, its widespread use is constrained by resource requirements and radiation exposure. Artificial intelligence-enabled electrocardiography (AI-ECG) may provide a complementary approach for CAD risk stratification. We developed and validated an AI-ECG model using CCTA as the reference standard to estimate severe ($\geq 70\%$) or complete ($\geq 99\%$) stenosis in the four major coronary arteries. In internal validation, the model achieved area under the receiver operating characteristic curve (AUC) values of 0.706–0.744 across vessels and demonstrated consistent performance in external validation (AUCs: 0.673–0.714). Discrimination remained stable among individuals with clinically normal ECGs and across demographic and clinical subgroups. In a dedicated clinical cohort with longitudinal follow-up, vessel-specific risk stratification based on model-predicted probabilities yielded distinct separation between high-risk and low-risk groups in time-to-event analyses using Kaplan–Meier curves, while decision curve analysis suggested potential clinical utility as an adjunctive screening tool. Explainable analyses highlighted waveform patterns associated with elevated predicted risk. These findings support the feasibility of AI-ECG for complementary CAD risk screening and warrant prospective evaluation.

Introduction

Coronary atherosclerotic heart disease (CAD) is one of the leading causes of death and disability worldwide, placing a heavy burden on public health systems and socioeconomic systems^{1–3}. Accurately identifying the responsible vessel in CAD, assessing lesion severity, and guiding individualized treatment decisions remain core challenges in clinical practice⁴.

Currently, coronary CT angiography (CCTA) is recommended as the first-line non-invasive modality for diagnosing CAD, providing a detailed assessment of coronary anatomy and stenosis severity, while serving as a crucial tool for pre-procedural planning and strategy guidance for

percutaneous coronary intervention (PCI)^{5,6}. Nevertheless, the widespread application of CCTA is limited by its dependence on advanced imaging infrastructure and post-processing techniques, strict requirements for heart rate control and respiratory coordination, radiation exposure, and the risk of contrast-induced nephropathy, particularly in patients with impaired renal function⁷⁻⁹. These limitations underscore the need for complementary, low-cost, and non-invasive approaches that can assist in CAD risk assessment and triage.

Electrocardiography (ECG), as a non-invasive, convenient, and real-time detection method, has unique advantages in the early identification and risk stratification of cardiovascular diseases. Changes in ECG waveforms, such as ST segment shift and T wave inversion, have been widely used in the preliminary diagnosis of acute coronary syndrome (ACS)¹⁰⁻¹². Meanwhile, with the rapid development of artificial intelligence (AI), especially deep learning technology, AI is being widely used in clinical research¹³⁻¹⁸. Utilizing AI to perform deep feature mining of ECG signals to predict the pathogenesis of cardiovascular diseases has become a research hotspot¹⁹⁻²³. However, existing AI-ECG studies on CAD-related coronary artery disease using CCTA mostly focus on whether there is screening for obstructive coronary artery disease. For example, Choi et al.'s study mainly targeted the detection of obstructive coronary artery disease²⁴, while Park et al.'s study focused on predicting obstructive lesions in patients with stable angina²⁵. Although some studies have attempted to use ECG and AI models to locate myocardial infarction (MI) sites, their research subjects are mostly scar tissue from previous MI, lacking systematic research on the localization of the responsible vessel during acute coronary syndrome and the identification of coronary artery occlusion on normal ECG²⁶.

To overcome these limitations, we conducted a multicenter study that included clinical data from Peking University People's Hospital and the Second Hospital of Tianjin Medical University, as well as a dedicated longitudinal follow-up cohort. We employed a transfer learning framework to fine-tune ECGFounder, a large-scale pretrained electrocardiogram foundation model^{27,28} which was adapted by our group on an independent dataset for MI-related prediction tasks, to develop an AI-ECG model capable of assessing severe stenosis and total occlusion of the four major coronary arteries as defined by coronary CT angiography (CCTA). Furthermore, we implemented vessel-specific risk stratification based on model-predicted probabilities and evaluated performance in individuals with clinically normal ECGs. To further explore the electrophysiological relevance underlying the model's predictions, we performed explainable analyses comparing waveform characteristics between high-risk and low-risk groups.

Overall, this study investigated the development and evaluation of an explainable artificial intelligence electrocardiogram (AI-ECG) model for the direct prediction of coronary computed tomography angiography (CCTA)-defined severe coronary artery stenosis and total occlusion from standard ECG signals. Model performance was systematically assessed using receiver operating characteristic analyses, comparisons of predicted probability distributions across different stenosis severities, and calibration analyses.

The model was further evaluated in individuals with apparently normal electrocardiograms to examine its behavior in populations without overt electrocardiographic abnormalities. In addition, model-predicted probabilities were integrated with epidemiological incidence data to perform vessel-specific risk stratification and to assess cumulative myocardial infarction risk over time using Kaplan–Meier analyses. Sensitivity analyses across a range of decision thresholds were conducted to explore operating points relevant to opportunistic screening scenarios. Finally, explainability analyses were performed to characterize differences in ECG waveform patterns between model-defined high-risk and low-risk groups, with the aim of supporting clinical interpretation.

Results

91

Baseline Character of Dataset

92

This study included multicenter clinical data from Peking University People's Hospital and the Second Hospital of Tianjin Medical University. Peking University People's Hospital included 2323 patients, comprising 2595 coronary CT angiography (CCTA) examinations and 4620 paired electrocardiogram (ECG) records; the Second Hospital of Tianjin Medical University included 2477 patients, comprising 2477 CCTA examinations and 2477 paired ECG records. Furthermore, we constructed a longitudinal follow-up cohort from the Second Hospital of Tianjin Medical University, including 400 patients, to evaluate the model's predictive ability in future risk stratification.

93

94

95

96

97

98

99

Data from Peking University People's Hospital was used as the internal dataset, and data from the Second Hospital of Tianjin Medical University was used as the external validation dataset to systematically evaluate the model's generalization performance in a multicenter scenario; the longitudinal follow-up cohort was used to validate the model's ability to stratify the risk of future adverse events (MI).

100

101

102

103

104

Table 1 shows the baseline characteristics of the data used in the study.

105

Development and Multi-Center Validation of AI-ECG Model

106

We employed a five-fold stratified cross-validation strategy with patient identifiers used as the grouping variable, ensuring that all ECG records from the same individual were assigned to a single fold and that the distribution of multi-label coronary artery outcomes was balanced across folds. To comprehensively evaluate model generalizability across multicenter datasets and its performance among individuals with clinically normal ECGs, we reported micro-averaged area under the receiver operating characteristic curve (micro-AUC) for the internal dataset, as well as performance on the external validation dataset using an ensemble of models derived from the five cross-validation folds. Model performance was additionally assessed in the subgroup of patients with clinically interpreted normal ECGs. Receiver operating characteristic (ROC) curves corresponding to these three evaluation settings are presented in Figure 1.

107

108

109

110

111

112

113

114

115

116

The results show that, in the internal validation set, the predicted AUCs for the right coronary artery (RCA), left main coronary artery (LM), left anterior descending artery (LAD), and left circumflex artery (LCX) are 0.744, 0.706, 0.716, and 0.736, respectively; while in the external validation set, the corresponding AUCs are 0.714, 0.713, 0.700, and 0.673. These results demonstrate that our AI-ECG model exhibits stable and superior discriminative performance in identifying severe stenosis and complete occlusion of the four major coronary arteries. The external validation results are generally consistent with the internal validation results, further confirming the model's good generalization ability across different central datasets.

117

118

119

120

121

122

123

124

Furthermore, we evaluated the model's predictive ability in the internal validation set for individuals with clinically normal ECGs. The results showed that in this subgroup, the predictive AUCs for RCA, LM, LAD, and LCX were 0.693, 0.659, 0.673, and 0.716, respectively. These results are largely consistent with the model's performance in the full population within the internal validation set, indicating that even in individuals with superficially normal ECGs, the AI-ECG model can effectively identify the potential risk of severe coronary artery stenosis, highlighting its potential application value in screening for occult CAD.

125

126

127

128

129

130

131

Meanwhile, we calculated the 95% confidence interval for the AUC index of each blood vessel. The range of this interval effectively reflects the statistical reliability and stability of the model's predictive performance, further supporting the credibility of the model's discriminative ability.

132

133

134

In addition, to account for potential differences between examination-level and patient-level

135

Table 1: Baseline Characteristics of Internal and External Datasets and Cohort

Characteristic	Peking University People's Hospital (Internal) (n = 4,620)	The Second Hospital of Tianjin Medical University (External) (n = 2,477)	Cohort of the Second Hospital of Tianjin Medical University (n = 400)
Demographics			
Sex			
Male	1,952 (42.3%)	1,283 (51.8%)	183 (45.8%)
Female	1,922 (41.6%)	1,194 (48.2%)	217 (54.2%)
Missing	746 (16.1%)	0 (0.0%)	0 (0.0%)
Age (years)			
Mean ± SD	64.5 ± 10.4	63.1 ± 11.7	63.14 ± 10.43
< 65	1,886 (40.8%)	1,223 (49.4%)	199 (49.8%)
≥ 65	1,988 (43.0%)	1,252 (50.5%)	201 (50.2%)
Missing	746 (16.1%)	2 (0.1%)	0 (0.0%)
Medical History			
Diabetes			
Yes	1,433 (31.0%)	889 (35.9%)	97 (24.3%)
No	3,187 (69.0%)	1,588 (64.1%)	303 (75.7%)
Hypertension			
Yes	2,411 (52.2%)	1,256 (50.7%)	171 (42.8%)
No	2,209 (47.8%)	1,221 (49.3%)	229 (57.2%)
Prior myocardial infarction			
Yes	193 (4.2%)	49 (2.0%)	16 (4.0%)
No	4,427 (95.8%)	2,428 (98.0%)	384 (96.0%)
Coronary Artery Stenosis			
RCA			
Severe stenosis & occlusion	795 (17.2%)	635 (25.6%)	64 (16.0%)
Non-severe or normal	3,825 (82.8%)	1,842 (74.4%)	336 (84.0%)
LM			
Severe stenosis & occlusion	235 (5.1%)	52 (2.1%)	4 (1.0%)
Non-severe or normal	4,385 (94.9%)	2,425 (97.9%)	396 (99.0%)
LAD			
Severe stenosis & occlusion	1,373 (29.7%)	769 (31.0%)	83 (20.8%)
Non-severe or normal	3,247 (70.3%)	1,708 (69.0%)	317 (79.2%)
LCX			
Severe stenosis & occlusion	795 (17.2%)	570 (23.0%)	55 (13.8%)
Non-severe or normal	3,825 (82.8%)	1,907 (77.0%)	345 (86.2%)

Data are presented as n (%) or mean ± SD.

Abbreviations: SD, standard deviation; RCA, right coronary artery; LM, left main coronary artery; LAD, left anterior descending artery; LCX, left circumflex artery.

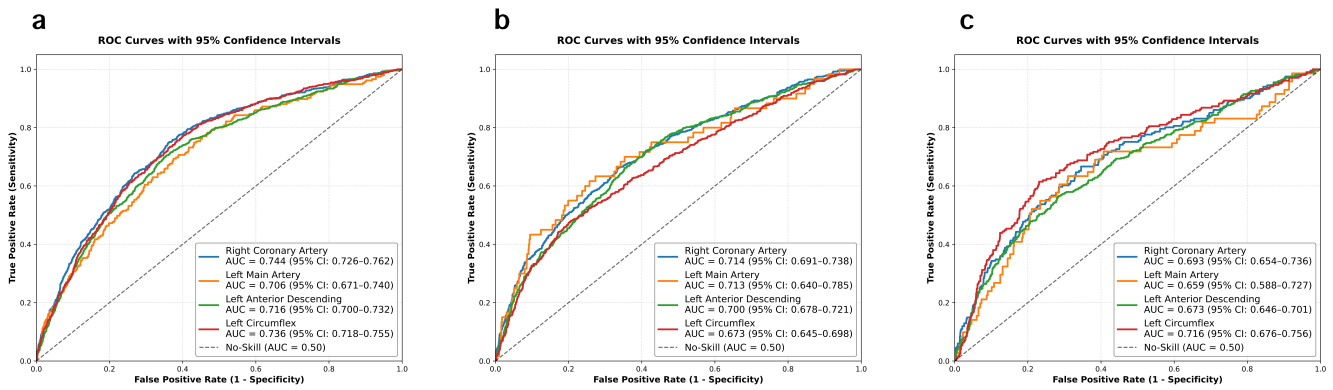


Figure 1: Model discrimination performance assessed by receiver operating characteristic curves. a) Internal validation using data from Peking University People’s Hospital. **b)** External validation using data from the Second Hospital of Tianjin Medical University. **c)** Performance evaluation in individuals with clinically normal electrocardiograms from the internal dataset. Area under the curve (AUC) values are reported with 95% confidence intervals (CI).

evaluation, ROC analyses were performed and reported at both the CCTA examination level and the patient level, with the corresponding curves shown in Figure 2. 136 137

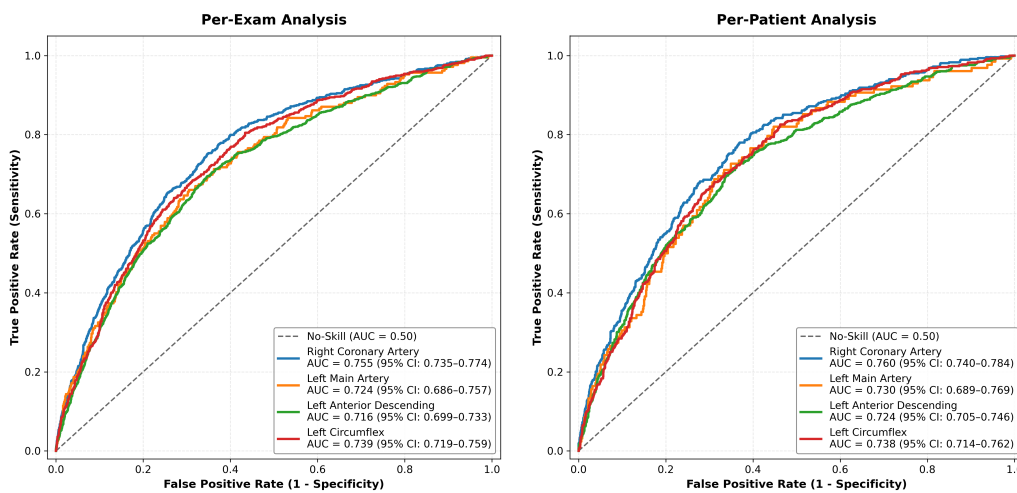


Figure 2: ROC analyses at the CCTA examination and patient levels. ROC curves are shown for model performance evaluated at both the CCTA examination level and the patient level, illustrating consistency of discrimination across different evaluation granularities.

Subgroup analyses were further performed to evaluate model stability across population characteristics and acquisition timing. After stratification by age ($< 65\text{years}$ vs. $\geq 65\text{years}$), sex, coronary artery stenosis, the interval between ECG and CCTA acquisition ($\leq 3\text{hours}$ vs. $> 3\text{hours}$), and the medical history, the model demonstrated largely comparable discriminative performance across subgroups, without evidence of substantial performance degradation. 138 139 140 141 142

As shown in Figure 3, model performance remained largely consistent across prespecified subgroups, with no substantial decline in area under the receiver operating characteristic curve (AUC) observed, except among individuals with a prior history of MI. 143 144 145

Specifically, higher AUC values were observed in the subgroup with an ECG–CCTA acquisition interval exceeding 3 hours, as well as among younger individuals (<65 years) and those with a history of hypertension. Model discrimination was comparable between male and female 146 147 148

participants and did not differ materially according to diabetes status.

Collectively, these findings suggest that the proposed model demonstrates stable discriminative performance across diverse population characteristics and testing conditions, supporting its potential applicability in heterogeneous clinical settings.

Subgroup analyses stratified by the severity of coronary artery stenosis are provided in Table A1.

To further validate the correlation between the model's predicted probabilities and the actual degree of stenosis, we plotted a box plot as shown in Figure 4. The box plot illustrates the predicted probability distribution of the four major coronary arteries at four degrees of stenosis (normal, mild, moderate, and severe). All vessels exhibit a consistent monotonically increasing trend, indicating that the model assigns a higher risk probability as the degree of stenosis increases.

Spearman rank correlation analysis confirmed a statistically significant positive correlation between the predicted probability and the degree of stenosis in all coronary arteries ($p < 0.001$), with the RCA showing the strongest correlation ($\rho = 0.371$). Notably, the absolute predicted probability of the left main coronary artery (LM) (range: 0.0–0.4) was significantly lower than that of other vessels, reflecting the low prevalence of LM lesions in the training population. However, the model still maintained significant discriminative power for LM ($\rho = 0.240$).

Model's Decision-making Ability in Coronary Artery Stenosis Risk Stratification

For the four major coronary arteries, this study established differentiated risk thresholds based on the epidemiological characteristics of severe stenosis and complete occlusion in each vessel, and divided patients into high-risk and low-risk groups based on model-predicted probabilities. Specifically, for LAD, LCX, and RCA, which have relatively high incidence rates, a predicted probability $\geq 15\%$ was defined as the high-risk threshold, referencing the pre-test probability stratification model proposed in the 2019 ESC guidelines. For LM, which has a significantly lower incidence rate, a predicted probability $\geq 1\%$ was set as the high-risk criterion based on an incidence rate enrichment strategy, in order to improve the sensitivity of identifying rare but clinically significant high-risk lesions.

To verify the reliability of the model's predictions, we plotted the model's prediction calibration curves on an internal dataset, as shown in Figure 5.

The calibration curves show that the model demonstrates good reliability in predicting all four coronary arteries. The Brier scores for RCA, LM, LAD, and LCX are 0.130, 0.047, 0.190, and 0.131, respectively. Notably, for severe and complete occlusion of the LM, the model did not output a very high prediction probability due to the extremely low incidence of this lesion in the general population (approximately 0.1%), which is consistent with epidemiological distribution.

To clearly demonstrate its performance, we magnified the LM subplot locally (between 0 and 0.35). The results show that although the predicted probabilities are concentrated in the low range, the high-risk group still exhibits a clear upward trend in risk, and the Brier Score (0.047) is extremely low, proving that the model has extremely high accuracy in excluding the vast majority of healthy people (High Negative Predictive Value), and does not produce a large number of false positives due to blindly pursuing high probabilities. The positive and negative rates of the experimental results are shown in Table A2.

To further evaluate the model's potential value in clinical risk stratification, we grouped patients based on model-predicted probabilities. Furthermore, we conducted a longitudinal comparison of the risk of myocardial infarction at different risk levels, as shown in Figure 6. The time of ECG acquisition was used as the start of follow-up, and an event was defined as a myocardial infarction

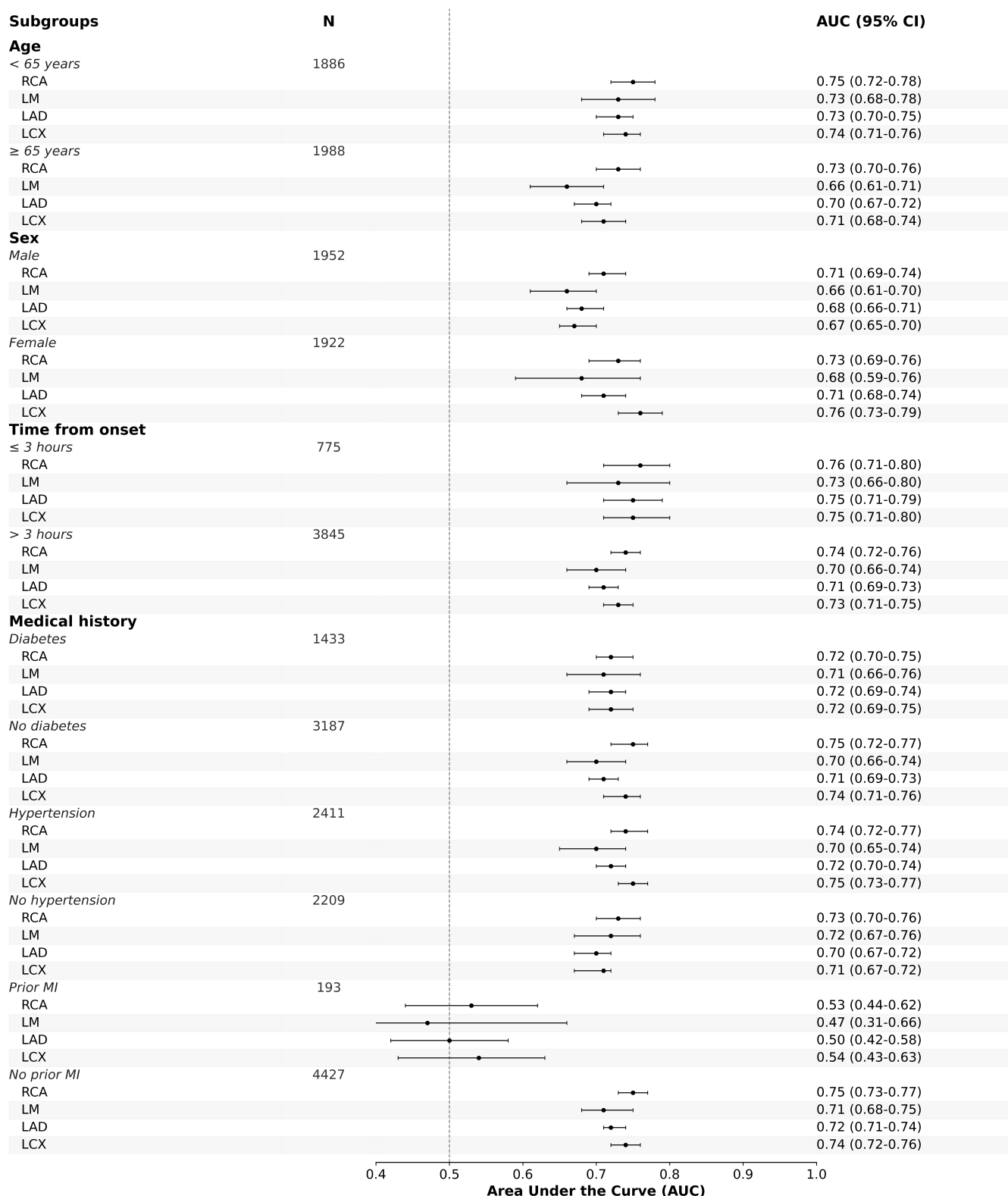


Figure 3: Subgroup analyses of model performance. Forest plots show the AUC with 95% CI across clinically relevant subgroups, including age, sex, time from symptom onset, and medical history.

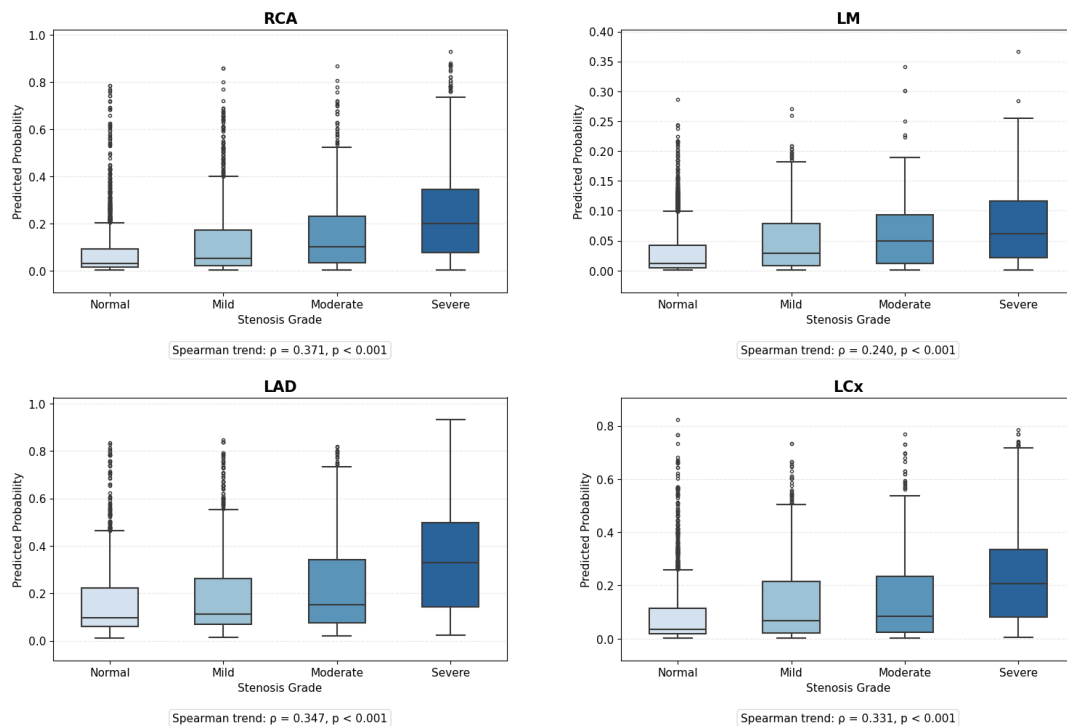


Figure 4: Distribution of model-predicted probabilities across different degrees of coronary stenosis. Box plots illustrate the predicted probability distributions for the four major coronary arteries (LAD, LCX, LM, and RCA) across four stenosis categories (normal, mild, moderate, and severe).

occurring during follow-up.

The analysis focused on incident events occurring within a predefined follow-up window of 700 days. Through Kaplan-Meier analysis, we compared the cumulative risk of myocardial infarction between the high-risk and low-risk groups during follow-up, thereby assessing the model’s ability to distinguish changes in future myocardial infarction risk over time.

As shown in Figure 6, Kaplan-Meier survival curves in all four major coronary arteries revealed a significant separation between high-risk and low-risk groups during follow-up. The cumulative incidence of myocardial infarction gradually increased over time, indicating a graded risk pattern in the risk stratification defined by the model. Log-rank tests showed statistically significant differences between risk groups in RCA ($p < 0.001$), LAD ($p = 0.029$), and LCX ($p = 0.002$). A trend of risk separation was also observed in the LM curve. In summary, these results demonstrate that the model can capture meaningful longitudinal risk stratification signals in major coronary arteries.

To evaluate the potential clinical utility of the proposed risk stratification strategy, we further conducted decision curve analysis (DCA) to quantify the net benefits of model-guided decision-making at different clinically relevant risk thresholds. As shown in Figure 7, in the four major coronary arteries, the DCA curves corresponding to the model are generally above the treat-all and treat-none strategies, indicating that model-based risk stratification can achieve higher net clinical benefits within the corresponding threshold ranges, supporting its potential application value as an auxiliary decision-making tool.

To further evaluate robustness, we examined model sensitivity and specificity across multiple alternative risk thresholds in addition to those used in the primary analysis. Performance remained consistent across a reasonable range of thresholds, indicating potential operating points for opportunistic screening (Figure A1 and Table A3).

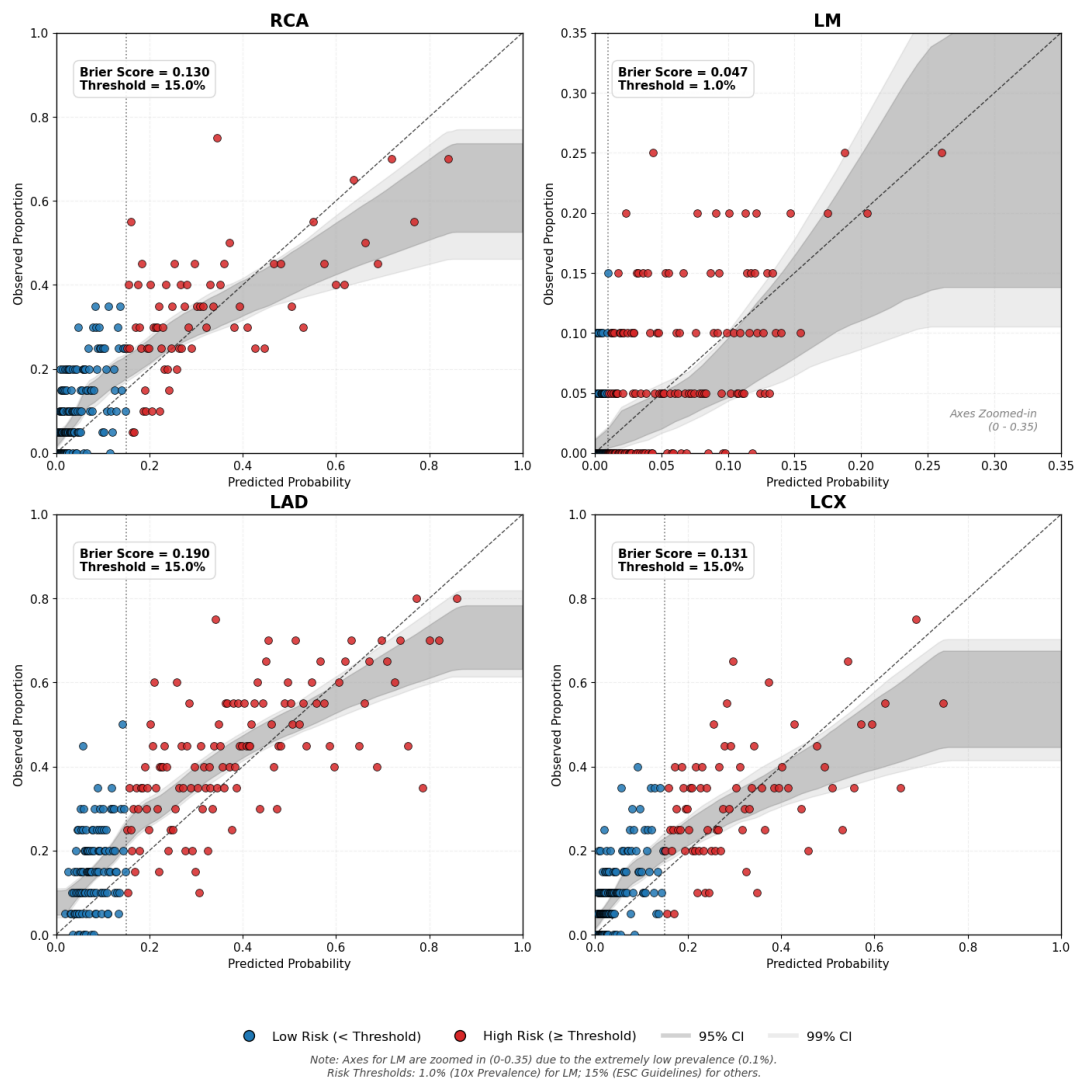


Figure 5: Calibration curve of model prediction results. Calibration plots illustrate the agreement between predicted and observed risks for each coronary artery. Red circles indicate individuals classified as the high-risk group, whereas blue circles indicate individuals classified as the low-risk group. All four coronary arteries demonstrated good calibration performance with low Brier scores.

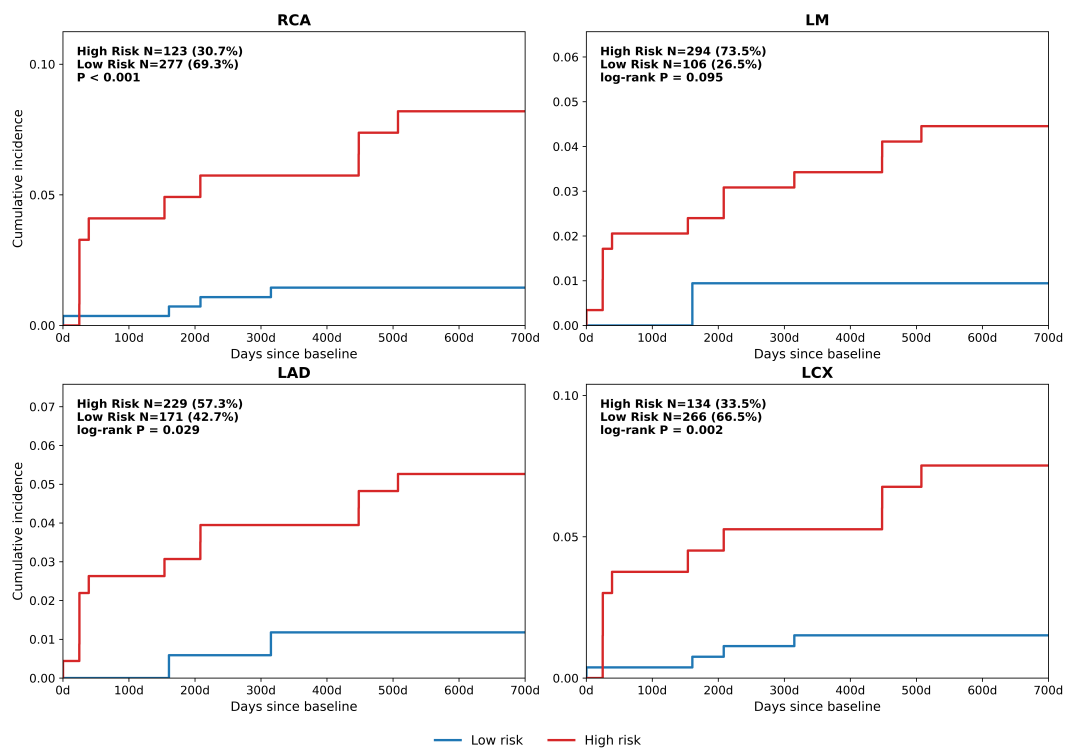


Figure 6: Kaplan–Meier curves stratified by model-predicted risk across major coronary arteries. Kaplan–Meier plots show the cumulative incidence of myocardial infarction over the follow-up period for individuals stratified into high-risk and low-risk groups based on model-predicted probabilities across the four major coronary arteries. Red solid lines represent the high-risk group, whereas blue solid lines represent the low-risk group.

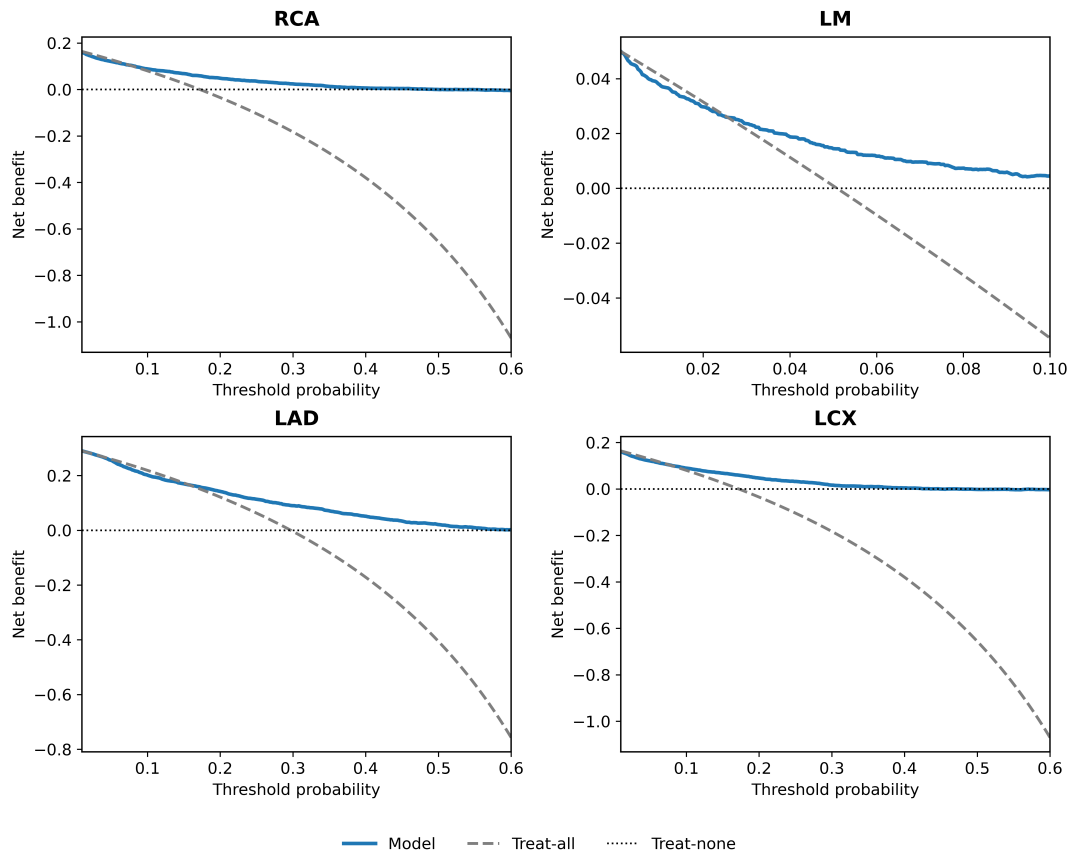


Figure 7: Decision curve analysis for model-guided coronary risk stratification. Decision curve analysis (DCA) illustrates the net clinical benefit of model-guided decision-making across a range of clinically relevant risk thresholds for the four major coronary arteries.

Explainability Analysis Results

220

To further elucidate the electrocardiographic regions contributing to model-based risk assessment and stratification, we performed an explainable analysis at the waveform level. Following stratification of the population into high-risk and low-risk groups based on model-predicted probabilities, individual heartbeat segments were extracted from raw ECG recordings, normalized, and temporally aligned. R-wave locations were identified on lead II using a peak detection algorithm, with predefined amplitude thresholds and a minimum RR interval to ensure robust detection of dominant QRS complexes. Using the detected R-wave as a reference point, standardized heartbeat waveforms were obtained for each individual. Within each risk group, the mean waveform morphology and corresponding standard deviation were computed for each lead and visualized in a multi-lead format to facilitate comparison between risk strata.

221

222

223

224

225

226

227

228

229

230

As shown in Figure 8, by comparing the differences in waveform morphology between high-risk and low-risk groups, the electrocardiographic feature patterns on which the model distinguishes different coronary artery risk states are intuitively revealed, providing explainable evidence for understanding its discrimination mechanism and potential electrophysiological basis.

231

232

233

234

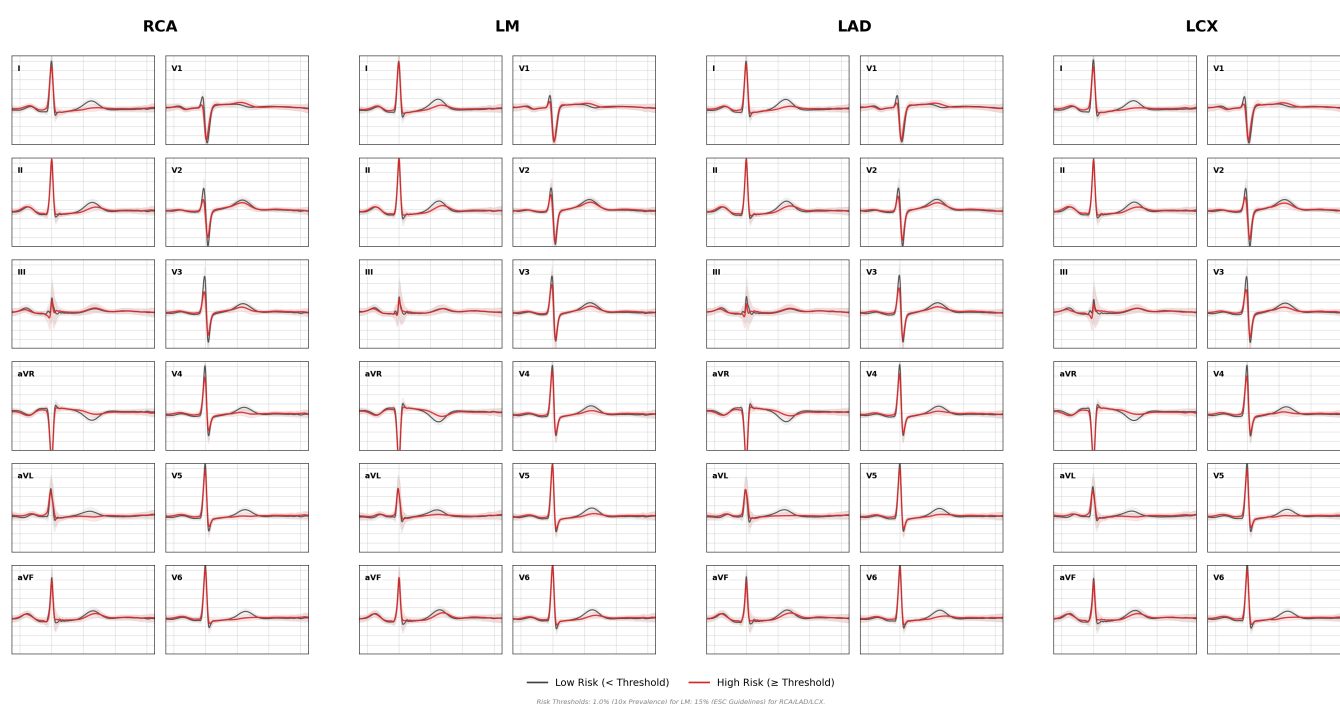


Figure 8: Explainable analysis results. The results reveal the key ECG regions that the model focuses on during prediction and stratification. Red lines indicate individuals classified as the high-risk group, whereas blue lines indicate individuals classified as the low-risk group.

Discussion

235

This study constructed and validated an ECG-based artificial intelligence model for predicting severe stenosis and total occlusion lesions shown by CCTA. Based on the large-scale pre-trained ECG foundation model ECGFounder, the model was further adapted to coronary artery disease-related tasks through transfer learning strategies, thereby expanding the application scope of existing AI-ECG studies in predicting outcome types and study populations.

236

237

238

239

240

The model's discriminative performance was systematically evaluated using multi-dimensional methods, including receiver operating characteristic (ROC) curve analysis, subgroup analysis,

241

242

and prediction probability distribution analysis, demonstrating stable performance under different population characteristics and testing conditions. 243

Furthermore, this study incorporated the epidemiological characteristics of different coronary artery lesions and used vessel-specific prediction probability thresholds to stratify the population at risk. The reliability and longitudinal discriminative power of the model's predictions were evaluated through calibration analysis and Kaplan-Meier curves. In addition, decision curve analysis showed that, within a range of clinically meaningful risk thresholds, the model-based risk stratification strategy had a higher net clinical benefit than the "treatment-all" and "treatment-none" strategies. Sensitivity analyses for different threshold selections also indicated that the model's performance remained stable within reasonable limits. 244

The main innovations of this study are reflected in the following aspects. First, the proposed model directly extracts clinically relevant information on severe stenosis and complete occlusion defined by CCTA from raw ECG signals, while maintaining stable performance in ECGs that are clinically interpreted as normal, highlighting its potential value for screening occult coronary artery disease. Second, the study systematically evaluated the model's ability for risk stratification, demonstrating its capacity to support clinical decision-making; in particular, decision curve analysis further demonstrates that model-assisted risk stratification can deliver net clinical benefit across a range of clinically relevant risk thresholds. Finally, by comparing ECG waveform characteristics between model-defined high-risk and low-risk populations, this study explored potential signal-level differences associated with coronary artery disease, providing a novel perspective for investigating its underlying electrophysiological mechanisms. 245

While this study demonstrates methodological innovation and explores the clinical applicability of AI-enabled ECG analysis for coronary artery disease, several limitations should be acknowledged. 246

First, the data were derived from two medical centers, and although multicenter validation was performed, further expansion in sample size and population diversity is necessary to strengthen generalizability across broader clinical settings. 247

Second, owing to the low incidence of severe and complete left main (LM) coronary obstruction, model performance for LM lesions was less stable in external validation and among individuals with clinically normal ECGs, suggesting that class imbalance may influence performance estimates and that these results should be interpreted with caution. 248

Third, the current study focuses on predicting CCTA-defined coronary stenosis from ECG signals, and the relationship between model performance and downstream clinical decision-making requires further investigation. In particular, how model-guided risk stratification may interact with different clinical management strategies remains to be explored through prospective studies. 249

Fourth, because the training and validation datasets excluded patients who had undergone percutaneous coronary intervention (PCI) or coronary artery bypass grafting (CABG), the applicability of the proposed model for evaluating in-stent restenosis or graft vessel occlusion after revascularization may be limited. In addition, the model showed reduced performance among individuals with a prior history of myocardial infarction, which may be attributable to persistent ECG alterations resulting from previous infarction that obscure lesion-specific electrophysiological patterns. Dedicated studies incorporating post-revascularization populations and patients with prior myocardial infarction are therefore warranted. 250

Fifth, the study population primarily reflects a real-world CCTA-referred cohort, in which patients with suspected acute myocardial infarction caused by complete coronary occlusion are typically triaged directly to invasive coronary angiography rather than CCTA. Consequently, detailed annotations distinguishing acute from chronic ischemic conditions were not consistently available, limiting the ability to differentiate electrophysiological patterns associated with acute versus chronic coronary occlusion. 251

Finally, although the explainable analyses provide insights into ECG regions contributing to model predictions, the clinical significance of subtle signal-level variations not readily discernible by human interpretation remains unclear. Moreover, current explainability approaches have inherent methodological limitations, underscoring the need for further methodological refinement. In future research, we plan to incorporate large-scale data from additional centers to further enhance the model's stability and generalizability. In parallel, we will conduct more refined analyses of LM coronary lesions, including the integration of spatial information from anterior and posterior ECG leads to better characterize electrocardiographic patterns associated with distinct anatomical regions and to improve lesion-specific identification. Importantly, to clarify the relationship between model performance and clinical decision-making, we are currently designing a prospective randomized controlled trial (RCT) to evaluate the impact of AI-ECG-guided risk stratification on downstream diagnostic strategies and clinical outcomes in real-world settings.

Methods

Overall Study Design and Methodological Framework

This study aimed to construct an AI-ECG model with explainable analysis capabilities to predict coronary artery lesions shown by CCTA based on ECG, thus providing a potential auxiliary tool for non-invasive risk assessment of CAD. The model was developed based on 2595 CCTA examinations and 4620 paired ECG data from 2323 patients at Peking University People's Hospital. To systematically evaluate the model's generalization ability across different centers and populations, we further validated it externally on 2477 CCTA examinations and 2477 paired ECG data from 2477 patients at the Second Hospital of Tianjin Medical University. In addition, this study included a longitudinal follow-up cohort of 400 patients from the Second Hospital of Tianjin Medical University to assess the model's prospective risk stratification ability in real-world clinical scenarios.

To comprehensively evaluate the model's clinical application potential, this study constructed a systematic performance evaluation framework, validating the model from multiple dimensions, including discriminative ability, predictive probability reliability, and clinical decision support value. First, ROC curves were plotted to evaluate the model's discriminative performance in identifying severe stenosis and total occlusion lesions shown by CCTA. Subsequently, by comparing the distribution of the model's predicted probabilities for different degrees of stenosis, the ability to differentiate the severity of coronary artery lesions was quantitatively analyzed. Based on this, the study subjects were divided into high-risk and low-risk groups by combining the model's predicted probabilities with the actual incidence of severe lesions. Simultaneously, calibration curves were used to systematically assess the reliability of model-predicted probabilities, while Kaplan–Meier analyses with log-rank tests were performed to evaluate the model's ability to stratify the risk of future MI events.

Furthermore, this study systematically analyzed the model's classification performance in subgroups based on age, sex, medical history, and the time interval between ECG and CCTA examinations. It further evaluated the model's ability to identify severe coronary artery stenosis in individuals with clinically normal ECGs, thus validating its potential value in screening for occult CAD. To avoid bias caused by different assessment granularities, we reported ROC analysis results at both the CCTA examination level and the patient level. Furthermore, to evaluate the model's application prospects in assisting clinical decision-making, this study plotted DCA curves and supplemented them with sensitivity analyses based on different risk thresholds. The aforementioned evaluation process covers multiple levels, from classification performance and

probabilistic reliability to clinical decision support potential, constructing a complete and coherent path for clinical performance validation of the model.

To enhance the explainability of the model results, this study further compared the differences in single-beat waveforms in 12-lead electrocardiograms across different risk groups identified by the model, analyzed key waveform regions emphasized by the model and their potential association with coronary artery lesions, and explored the model's discriminative criteria from an electrophysiological perspective. This analysis provides intuitive evidence for understanding the working mechanism of artificial intelligence electrocardiography in coronary artery disease identification and offers a new research perspective for related clinical and methodological studies.

Data Sources and Labeling Strategy

This study included data from 2323 patients at Peking University People's Hospital for model development, encompassing 2595 coronary CT angiography (CCTA) examinations and 4620 paired electrocardiogram (ECG) recordings. These patients were identified after applying predefined exclusion criteria, whereby individuals with evidence of prior or subsequent percutaneous coronary intervention (PCI) or coronary artery bypass grafting (CABG) related to the indexed CCTA were excluded. External validation was performed using data from 2477 patients at the Second Hospital of Tianjin Medical University, including 2477 CCTA examinations and 2477 paired ECG records, after applying the same exclusion criteria. In addition, a longitudinal follow-up cohort comprising 400 patients from the Second Hospital of Tianjin Medical University was constructed to evaluate the model's risk stratification capability during clinical follow-up.

To further minimize the potential influence of coronary revascularization procedures on ECG characteristics, all ECG recordings were required to precede the corresponding CCTA examination. This combined temporal and clinical exclusion strategy was adopted to reduce bias introduced by procedure-related ECG alterations.

The study was approved by the Peking University Medical Ethics Committee (Approval No.: IRB00001052-23071), Peking University People's hospital Ethics Committee (Approval No.: 2024PHB428-001), and the ethical review committee of The Second Hospital of Tianjin Medical University (Approval No.: KY2025K386). And the requirement for informed consent was waived in accordance with relevant ethical guidelines.

Based on CCTA examination reports, under the supervision of professional clinicians, a large language model was used to perform structured parsing, cleaning, and standardization of the original imaging diagnostic text to systematically extract stenosis information for the right coronary artery (RCA), left anterior descending artery (LAD), left circumflex artery (LCX), and left main coronary artery (LM). According to clinically accepted standards, luminal stenosis was categorized as normal (<25%), mild stenosis (25–50%), moderate stenosis (50–70%), severe stenosis ($\geq 70\%$), or complete occlusion. For model development and evaluation, lesions classified as normal, mild stenosis, or moderate stenosis were grouped as non-severe stenosis, whereas severe stenosis and complete occlusion were grouped as severe lesions. All label generation and cleaning processes underwent manual auditing and confirmation by multiple clinicians to ensure consistency and reliability. This stratification scheme is consistent with clinical practice for identifying coronary artery lesions with established prognostic significance.

Simultaneously, the ECG diagnostic texts were uniformly cleaned and recoded, and the study population was further divided into two categories: "normal ECG" and "abnormal ECG," to support subsequent stratified analysis of the ability to identify occult coronary artery lesions. All ECG classifications were audited by clinicians.

Model Architecture and Training Strategy

383

This study fine-tuned the ECGFounder model trained for future new-onset MI using a transfer learning strategy^{27,28}. An AI-ECG model based on a multi-task deep learning framework was constructed to jointly predict severe stenosis and complete occlusion of four major coronary arteries (RCA, LM, LAD, LCX). The model uses a Net1D network structure with 12-lead ECG signals as input.

384

385

386

387

388

To address the gradient conflict and weight imbalance issues between different tasks during multi-task learning, an adaptive weighting strategy based on task uncertainty was introduced²⁹. Specifically, for each task t , the loss function was weighted by a learnable uncertainty parameter σ_t , and the overall objective was defined as:

389

390

391

392

$$\mathcal{L} = \sum_{t=1}^T \left(\frac{1}{2\sigma_t^2} \mathcal{L}_t + \log \sigma_t \right), \quad (1)$$

where \mathcal{L}_t denotes the task-specific loss and σ_t represents the task uncertainty, which is optimized jointly with model parameters. This formulation enables dynamic balancing of multiple tasks during training.

393

394

395

In addition, the Projected Conflicting Gradient (PCGrad) algorithm was applied to further mitigate gradient interference between tasks³⁰. For two task gradients g_i and g_j , when their dot product is negative, indicating conflicting optimization directions, the gradient was adjusted as:

396

397

398

$$g_i \leftarrow g_i - \frac{g_i^\top g_j}{\|g_j\|^2} g_j, \quad \text{if } g_i^\top g_j < 0, \quad (2)$$

thereby projecting conflicting gradients onto a non-conflicting direction to improve convergence stability.

399

400

The optimization process employed the AdamW optimizer combined with warmup and cosine decay strategies to dynamically adjust the learning rate, enhancing training robustness and generalization performance.

401

402

403

Data partitioning employed a five-fold stratified grouped cross-validation method, using patient ID as the grouping criterion to ensure that data from the same patient did not appear simultaneously in both the training and validation sets, while maintaining the balance of multi-label distribution. The model used the validation set Macro-AUC as the primary performance monitoring metric, and the weights of the best-performing model in each fold were stored.

404

405

406

407

408

After reading the 12-lead ECG signal, lead-by-lead z-score standardization was first performed to eliminate the impact of inter-individual amplitude differences on model training. To enhance the model's robustness to signal perturbations encountered in real-world clinical scenarios, an online data augmentation strategy was employed during training to generate augmented ECG samples via controlled random perturbations.

409

410

411

412

413

Specifically, each ECG signal was subjected to stochastic transformations, including random temporal shifting, amplitude scaling, additive Gaussian noise injection, and local random occlusion. Temporal shifting was implemented by rolling the signal along the time axis within a range of $\pm 10\%$ of the signal length, simulating beat misalignment. Amplitude scaling was performed by multiplying the signal with a random factor sampled from a uniform distribution in the range $[0.9, 1.1]$, mimicking inter-beat voltage variation. Gaussian noise with zero mean and variance proportional to the augmentation intensity was added to emulate physiological and acquisition noise, while local random occlusion was applied by setting a contiguous segment (2%–10% of signal length) to zero, simulating signal dropout or artifact interference.

414

415

416

417

418

419

420

421

422

The augmentation strength was modulated by an epoch-dependent cosine annealing function:

423

$$\alpha(e) = 0.5 + 0.5 \cos \left(\frac{\pi e}{E} \right), \quad (3)$$

where e denotes the current training epoch and E represents the total number of training epochs. This formulation ensured that augmentation intensity gradually decreased from 1.0 to 0.5 throughout training, enabling the model to initially learn robust invariant representations under strong perturbations and subsequently focus on stable morphological features in later stages, thereby improving generalization while avoiding excessive distortion of physiologically relevant ECG patterns.

During training, both the original ECG signal and its augmented counterpart were simultaneously fed into the network, encouraging the model to learn consistent representations across perturbed signal variations.

The training strategy described above, while ensuring data isolation at the patient level, enables the model to make stable joint predictions of multivascular lesions and further outputs continuous probability results, providing a methodological basis for subsequent risk stratification analysis, calibration assessment and clinical decision support.

Evaluation Methods

To systematically evaluate the predictive performance of the model, the ROC curves were plotted in both internal and external validation sets, and the 95% confidence intervals for each AUC were calculated to quantify the classification and discrimination capabilities of the model.

Based on different true diagnostic categories in CCTA, box plots of the model's predicted probabilities for corresponding patients were generated, and the Spearman rank correlation test was used to assess the trend relationship between different coronary artery stenosis grades and the model's predicted probabilities. By encoding the stenosis degree into ordered numerical codes ("no obvious stenosis, mild stenosis, moderate stenosis, severe stenosis"), the monotonic correlation between these codes and the model's output probability was analyzed to determine whether the model's predicted probability showed a significant upward trend with increasing stenosis degree, thus validating the model's discriminative power and reliability from a probability distribution perspective.

Furthermore, we conducted subgroup analyses on the internal validation set, stratifying the population based on age (< 65 years vs. ≥ 65 years), sex, medical history, and the time interval between ECG and CCTA examinations (≤ 3 hours vs. > 3 hours). We systematically compared the differences in model performance among different subgroups to assess the model's robustness under various population characteristics and time conditions. Finally, for patients with normal ECG diagnoses, we further analyzed the model's prediction results to validate the potential application value in detecting occult CAD. Furthermore, we analyzed the data on exam-level and patient-level data to verify the robustness of the model.

Clinical Risk Stratification

Based on the differences in the incidence of the four major coronary arteries (LAD, LCX, LM, RCA) in the real-world population, we divided the vessels into two groups: relatively high incidence and extremely low incidence, to set differentiated model prediction thresholds. Referring to the results of Bergström et al.'s study based on the large-scale SCAPIS cohort ($n = 25,182$), the anatomical distribution of significant coronary artery stenosis differs greatly in the general population without known coronary artery disease³¹. Specifically, the probability of significant stenosis in the LM is extremely low, only 0.1%; in contrast, the incidence in other major vessels is approximately 20 times higher (1.9%) than in the LM. Based on this significant epidemiological difference, we grouped LAD, LCX, and RCA into the relatively high incidence group, while classifying the LM separately into the extremely low incidence group.

For blood vessels with high incidence (LAD, LCX, RCA), referring to the pre-test probability (PTP) model based on a pooled analysis of contemporary large-scale patient cohorts in the 2019 ESC guidelines, a predicted probability of $\geq 15\%$ from the AI-ECG model was defined as high risk³². For LM with extremely low incidence, considering its extremely low baseline incidence in the general population (0.1%), we adopted an incidence enrichment strategy, defining a predicted risk of 10 times the baseline incidence (i.e., $\geq 1.0\%$) as high risk³³. Although this threshold is low in absolute value, it represents a highly significant relative risk ($RR = 10$), aiming to significantly reduce the number of people requiring screening (NNS) in clinical screening, thereby improving diagnostic benefits.

Explainability Analysis

The study stratifies patients according to predicted probabilities in the model and further compares the characteristic differences in the ECG waveforms between different risk groups to improve the explainability of the AI-ECG model and reveal the electrophysiological basis of its risk assessment.

Specifically, based on the predicted probabilities corresponding to each coronary arteries and preset risk thresholds, the population is divided into high-risk and low-risk groups. R waves are then automatically detected from the raw ECG signals of each patient, and individual heartbeats are time-aligned to extract standardized heartbeat segments, which are then normalized by z-score for each lead. The heartbeat waveforms within different risk groups are summarized and calculated to obtain the average waveform and standard deviation for each lead, and visualized using a multi-lead grid.

By comparing the morphological differences in key electrophysiological features such as P waves, QRS complexes, and ST-T segments between high-risk and low-risk individuals, the waveform patterns relied upon by the model to distinguish different coronary artery risk states are intuitively revealed, thus providing intuitive evidence for understanding the model's decision-making mechanism and its underlying physiological basis.

Declaration statements

Data Availability

The data that support the findings of this study are not publicly available due to restrictions imposed by institutional ethics committees and data governance policies of the participating hospitals. Access to the data may be considered upon reasonable request to the corresponding author, subject to approval by the relevant ethics committees.

Code Availability

The code used for model development and evaluation in this study is publicly available at <https://github.com/shunxio/AnyECG-CCTA>.

Acknowledgements

Shenda Hong is supported by the National Natural Science Foundation of China (62102008, 62172018), the CCF–Tencent Rhino-Bird Open Research Fund (CCF-Tencent RAGR20250108), the CCF–Zhipu Large Model Innovation Fund (CCF-Zhipu202414), the PKU–OPPO Fund (BO202301, BO202503), and the Research Project of Peking University in the State Key Laboratory of Vascular

Homeostasis and Remodeling (2025-SKLVHR-YCTS-02). Kangyin Chen is supported by the National Natural Science Foundation of China (82470527). The authors thank all collaborators and participating institutions for their support and contributions to this research.

Author Contributions

Yujie Xiao led the conceptualization of the study, designed the methodology, implemented the models, performed validation and formal analyses, and drafted the initial version of the manuscript. Qinghao Zhao contributed to the manuscript revision process, assisted in refining the explanation of results, and provided critical feedback on the study. Jian Liu, Hao Zhang and Tong Liu contributed to data acquisition, preprocessing, and curation. Gongzheng Tang, Zhuoran Kan, Deyun Zhang, Jun Li, Guangkun Nie, Xiaocheng Fang, Haoyu Wang, and Shun Huang contributed to data preparation and investigation. Kangyin Chen provided clinical expertise and contributed to data interpretation. Shenda Hong supervised the entire project, provided resources, guided study design and interpretation, served as the corresponding author, and takes full responsibility for the integrity of the work. All authors reviewed, revised, and approved the final manuscript.

Competing Interests

Shenda Hong is an Associate Editor of *npj Digital Medicine*. Shenda Hong was not involved in the journal's review of, or decisions related to, this manuscript. The other authors declare no competing financial or non-financial interests.

References

1. Martin, S.S., Aday, A.W., Almarzooq, Z.I., Anderson, C.A., Arora, P., Avery, C.L., Baker-Smith, C.M., Barone Gibbs, B., Beaton, A.Z., Boehme, A.K. et al. (2024). 2024 heart disease and stroke statistics: a report of us and global data from the american heart association. *Circulation* 149, e347–e913.
2. Mensah, G.A., Fuster, V., Murray, C.J., Roth, G.A., of Cardiovascular Diseases, G.B., and Collaborators, R. (2023). Global burden of cardiovascular diseases and risks, 1990-2022. *Journal of the American College of Cardiology* 82, 2350–2473.
3. Luengo-Fernandez, R., Walli-Attaei, M., Gray, A., Torbica, A., Maggioni, A.P., Huculeci, R., Bairami, F., Aboyans, V., Timmis, A.D., Vardas, P. et al. (2023). Economic burden of cardiovascular diseases in the european union: a population-based cost study. *European heart journal* 44, 4752–4767.
4. Vrints, C., Andreotti, F., Koskinas, K.C., Rossello, X., Adamo, M., Ainslie, J., Banning, A.P., Budaj, A., Buechel, R.R., Chiariello, G.A. et al. (2024). 2024 esc guidelines for the management of chronic coronary syndromes: developed by the task force for the management of chronic coronary syndromes of the european society of cardiology (esc) endorsed by the european association for cardio-thoracic surgery (eacts). *European heart journal* 45, 3415–3537.
5. Kim, C., Park, C.H., Lee, B.Y., Park, C.H., Kang, E.J., Koo, H.J., Kitagawa, K., Cha, M.J., Krittayaphong, R., Choi, S.I. et al. (2024). 2024 consensus statement on coronary stenosis and plaque evaluation in ct angiography from the asian society of cardiovascular imaging-practical tutorial (asci-pt). *Korean journal of radiology* 25, 331.

6. Members, W.C., Gulati, M., Levy, P.D., Mukherjee, D., Amsterdam, E., Bhatt, D.L., Birtcher, K.K., Blankstein, R., Boyd, J., Bullock-Palmer, R.P. et al. (2021). 2021 aha/acc/ase/cest/saem/scct/scmr guideline for the evaluation and diagnosis of chest pain: a report of the american college of cardiology/american heart association joint committee on clinical practice guidelines. *Journal of the American College of Cardiology* 78, e187–e285. 548
549
550
551
552
7. Narula, J., Chandrashekar, Y., Ahmadi, A., Abbara, S., Berman, D.S., Blankstein, R., Leipsic, J., Newby, D., Nicol, E.D., Nieman, K. et al. (2020). Scct 2021 expert consensus document on coronary computed tomographic angiography: a report of the society of cardiovascular computed tomography. *Journal of cardiovascular computed tomography* 15, 192. 553
554
555
556
8. Yu, H., Song, H., Sun, X., Song, T., Xie, A., Xu, J., Qin, R., Jing, L., Zuo, T., Zhao, J. et al. (2024). Reduced radiation dose and volume of contrast medium in heart rate-based, one-stop computed tomography angiography of coronary, carotid and cerebrovascular arteries. *Acta Radiologica* 65, 84–90. 557
558
559
560
9. Jain, S., and Majidi, F. (2025). Ct coronary angiography vs cardiac catheterization and risk of acute kidney injury—comparative study. *Journal of Clinical Cardiology* 6, 84–90. 561
562
10. Byrne, R.A., Rossello, X., Coughlan, J., Barbato, E., Berry, C., Chieffo, A., Claeys, M.J., Dan, G.A., Dweck, M.R., Galbraith, M. et al. (2024). 2023 esc guidelines for the management of acute coronary syndromes: developed by the task force on the management of acute coronary syndromes of the european society of cardiology (esc). *European Heart Journal: Acute Cardiovascular Care* 13, 55–161. 563
564
565
566
567
11. Bhatt, D.L., Lopes, R.D., and Harrington, R.A. (2022). Diagnosis and treatment of acute coronary syndromes: a review. *Jama* 327, 662–675. 568
569
12. Thygesen, K., Alpert, J.S., Jaffe, A.S., Chaitman, B.R., Bax, J.J., Morrow, D.A., White, H.D., and on behalf of the Joint European Society of Cardiology (ESC)/American College of Cardiology (ACC)/American Heart Association (AHA)/World Heart Federation (WHF) Task Force for the Universal Definition of Myocardial Infarction, E.G. (2018). Fourth universal definition of myocardial infarction (2018). *Journal of the American college of cardiology* 72, 2231–2264. 570
571
572
573
574
575
13. Zhao, Q., Geng, S., Wang, B., Sun, Y., Nie, W., Bai, B., Yu, C., Zhang, F., Tang, G., Zhang, D. et al. (2024). Deep learning in heart sound analysis: from techniques to clinical applications. *Health Data Science* 4, 0182. 576
577
578
14. Luo, Y., Liu, X.Y., Yang, K., Huang, K., Hong, M., Zhang, J., Wu, Y., and Nie, Z. (2024). Toward unified ai drug discovery with multimodal knowledge. *Health Data Science* 4, 0113. 579
580
15. Zhang, S., Mu, W., Dong, D., Wei, J., Fang, M., Shao, L., Zhou, Y., He, B., Zhang, S., Liu, Z. et al. (2023). The applications of artificial intelligence in digestive system neoplasms: a review. *Health Data Science* 3, 0005. 581
582
583
16. Tham, Y.C., Goh, J.H.L., Anees, A., Lei, X., Rim, T.H., Chee, M.L., Wang, Y.X., Jonas, J.B., Thakur, S., Teo, Z.L. et al. (2022). Detecting visually significant cataract using retinal photograph-based deep learning. *Nature aging* 2, 264–271. 584
585
586
17. Liu, X., Gao, K., Liu, B., Pan, C., Liang, K., Yan, L., Ma, J., He, F., Zhang, S., Pan, S. et al. (2021). Advances in deep learning-based medical image analysis. *Health Data Science* 2021, 8786793. 587
588
589

18. Xiao, Y., Tang, G., Liu, W., Li, J., Nie, G., Kan, Z., Zhang, D., Zhao, Q., and Hong, S. (2025). Anyecg-lab: An exploration study of fine-tuning an ecg foundation model to estimate laboratory values from single-lead ecg signals. *arXiv preprint arXiv:2510.22301*. 590
591
592
19. Croon, P.M., Dhingra, L.S., Biswas, D., Oikonomou, E.K., and Khera, R. (2025). Phenotypic selectivity of artificial intelligence-enhanced electrocardiography in cardiovascular diagnosis and risk prediction. *Circulation* 152. 593
594
595
20. Poterucha, T.J., Jing, L., Ricart, R.P., Adjei-Mosi, M., Finer, J., Hartzel, D., Kelsey, C., Long, A., Rocha, D., Ruhl, J.A. et al. (2025). Detecting structural heart disease from electrocardiograms using ai. *Nature* 644, 221–230. 596
597
598
21. Yang, K., Hong, M., Zhang, J., Luo, Y., Zhao, S., Zhang, O., Yu, X., Zhou, J., Yang, L., Zhang, P. et al. (2025). Ecg-lm: Understanding electrocardiogram with a large language model. *Health Data Science* 5, 0221. 599
600
601
22. Al-Zaiti, S.S., Martin-Gill, C., Zègre-Hemsey, J.K., Bouzid, Z., Faramand, Z., Alrawashdeh, M.O., Gregg, R.E., Helman, S., Riek, N.T., Kraevsky-Phillips, K. et al. (2023). Machine learning for ecg diagnosis and risk stratification of occlusion myocardial infarction. *Nature Medicine* 29, 1804–1813. 602
603
604
605
23. Lin, C.S., Liu, W.T., Tsai, D.J., Lou, Y.S., Chang, C.H., Lee, C.C., Fang, W.H., Wang, C.C., Chen, Y.Y., Lin, W.S. et al. (2024). Ai-enabled electrocardiography alert intervention and all-cause mortality: a pragmatic randomized clinical trial. *Nature Medicine* 30, 1461–1470. 606
607
608
24. Choi, S.H., Lee, H.G., Park, S.D., Bae, J.W., Lee, W., Kim, M.S., Kim, T.H., and Lee, W.K. (2023). Electrocardiogram-based deep learning algorithm for the screening of obstructive coronary artery disease. *BMC cardiovascular disorders* 23, 287. 609
610
611
25. Park, J., Kim, J., Kang, S.H., Lee, J., Hong, Y., Chang, H.J., Cho, Y., and Yoon, Y.E. (2024). Artificial intelligence-enhanced electrocardiography analysis as a promising tool for predicting obstructive coronary artery disease in patients with stable angina. *European Heart Journal-Digital Health* 5, 444–453. 612
613
614
615
26. Wang, H., Gao, Z., Zhang, H., Zhu, Y., Lian, S., Bo, K., Li, S., Gao, Y., Zhuang, B., Zhou, Z. et al. (2025). Artificial intelligence-based accurate myocardial infarction mapping using 12-lead electrocardiography. *European Heart Journal-Digital Health* pp. ztaf077. 616
617
618
27. Hong, S., Xu, Y., Khare, A., Priambada, S., Maher, K., Aljiffry, A., Sun, J., and Tumanov, A. (2020). Holmes: health online model ensemble serving for deep learning models in intensive care units. In *Proceedings of the 26th ACM SIGKDD International Conference on Knowledge Discovery & Data Mining*. pp. 1614–1624. 619
620
621
622
28. Li, J., Aguirre, A.D., Junior, V.M., Jin, J., Liu, C., Zhong, L., Sun, C., Clifford, G., Brandon Westover, M., and Hong, S. (2025). An electrocardiogram foundation model built on over 10 million recordings. *NEJM AI* 2, Aloa2401033. 623
624
625
29. Kendall, A., Gal, Y., and Cipolla, R. (2018). Multi-task learning using uncertainty to weigh losses for scene geometry and semantics. In *Proceedings of the IEEE conference on computer vision and pattern recognition*. pp. 7482–7491. 626
627
628
30. Yu, T., Kumar, S., Gupta, A., Levine, S., Hausman, K., and Finn, C. (2020). Gradient surgery for multi-task learning. *Advances in neural information processing systems* 33, 5824–5836. 629
630

31. Bergström, G., Persson, M., Adiels, M., Björnson, E., Bonander, C., Ahlström, H., Alfredsson, J., Angerås, O., Berglund, G., Blomberg, A. et al. (2021). Prevalence of subclinical coronary artery atherosclerosis in the general population. *Circulation* *144*, 916–929. 631
632
633
32. Knuuti, J., Wijns, W., Saraste, A., Capodanno, D., Barbato, E., Funck-Brentano, C., Prescott, E., Storey, R.F., Deaton, C., Cuisset, T. et al. (2020). 2019 esc guidelines for the diagnosis and management of chronic coronary syndromes: The task force for the diagnosis and management of chronic coronary syndromes of the european society of cardiology (esc). *European heart journal* *41*, 407–477. 634
635
636
637
638
33. Temple, R. (2010). Enrichment of clinical study populations. *Clinical Pharmacology & Therapeutics* *88*, 774–778. 639
640